Appl. Math. Mech. -Engl. Ed., **41**(12), 1897–1914 (2020)

APPLIED MATHEMATICS AND MECHANICS (ENGLISH EDITION)

https://doi.org/10.1007/s10483-020-2674-6

Meshless acoustic analysis using a weakly singular Burton-Miller boundary integral formulation*

Linchong CHEN[1], Xiaolin LI[2,†]

1. School of Mathematics and Information Engineering, Chongqing University of Education, Chongqing 400065, China;
2. School of Mathematical Sciences, Chongqing Normal University, Chongqing 400047, China;

(Received Feb. 26, 2020 / Revised Jul. 30, 2020)

Abstract The Burton-Miller boundary integral formulation is solved by a complex variable boundary element-free method (CVBEFM) for the boundary-only meshless analysis of acoustic problems with arbitrary wavenumbers. To regularize both strongly singular and hypersingular integrals and to avoid the computation of the solid angle and its normal derivative, a weakly singular Burton-Miller formulation is derived by considering the normal derivative of the solid angle and adopting the singularity subtraction procedures. To facilitate the implementation of the CVBEFM and the approximation of gradients of the boundary variables, a stabilized complex variable moving least-square approximation is selected in the meshless discretization procedure. The results show the accuracy and efficiency of the present CVBEFM and reveal that the method can produce satisfactory results for all wavenumbers, even for extremely large wavenumbers such as $k = 10\,000$.

Key words meshless method, complex variable moving least-square approximation, boundary element-free method, Burton-Miller formulation, regularization, high frequency acoustic problem, large wavenumber

Chinese Library Classification O241.8
2010 Mathematics Subject Classification 65N38

1 Introduction

The numerical analysis of acoustic problems has various applications in many scientific fields[1]. In recent years, various meshless methods, such as the singular meshless method[2], the boundary point interpolation method[3], the singular boundary method[4], the localized method of fundamental solutions[5], the localized boundary knot method[6], the local radial

* Citation: CHEN, L. C. and LI, X. L. Meshless acoustic analysis using a weakly singular Burton-Miller boundary integral formulation. *Applied Mathematics and Mechanics* (*English Edition*), **41**(12), 1897–1914 (2020) https://doi.org/10.1007/s10483-020-2674-6

† Corresponding author, E-mail: lxlmath@163.com

Project supported by the National Natural Science Foundation of China (No. 11971085), the Innovation Research Group Project in Universities of Chongqing of China (No. CXQT19018), the Science and Technology Research Program of Chongqing Municipal Education Commission of China (No. KJZD-M201800501), and the Science and Technology Research Program of Chongqing University of Education of China (No. KY201927C)

point interpolation method[7], the Galerkin meshfree method[8], and the element-free Galerkin method[9], have been applied to acoustic problems. Boundary integral equations (BIEs)[1,10] are powerful and popular for the numerical solutions of acoustic problems, since they reduce the problem dimensionality and fulfill the radiation condition at infinity in a nature way. Boundary element methods (BEMs)[1] and boundary-type meshless methods[2–4,11] possess significant advantages over domain-type methods such as the finite element method for acoustic problems, especially with unbounded domains.

Different from the BIEs for Laplace and elasticity problems, the BIEs for exterior acoustic problems may fail to offer unique solutions at some characteristic wavenumbers of the associated interior problem. Various techniques have been developed to circumvent this annoying shortcoming successfully. The well-known Burton-Miller formulation[12] presents a direct BIE method by using a linear combination of the singular BIE and the associated hypersingular BIE, while the combined field integral equation (CFIE)[13–14] presents an indirect BIE method by using a combination of single and double layer potentials. The applications of the CFIE have been studied mainly to acoustic problems with Dirichlet boundary conditions, rarely to problems with Neumann conditions, and none to problems with mixed conditions[13–14]. In the case of using the CFIE, the computational formulae for Dirichlet and Neumann problems are different, and cannot be unified.

It has been proven theoretically and verified numerically that the Burton-Miller formulation can obtain unique solutions for exterior acoustic problems with arbitrary wavenumbers. The applications of the Burton-Miller formulation have been studied extensively by the BEM[15–17]. Although numerous reported studies indicate that BIE-based meshless methods perform excellently in solving boundary value problems such as Laplace and elasticity problems[18], very few applications of the Burton-Miller formulation to BIE-based meshless methods have been found.

The boundary element-free method (BEFM)[18] is a promising BIE-based meshless method. It not only alleviates the meshing-related shortcomings, but also enhances the precision of BEMs. With the aid of the singular BIE, the BEFM can be applied to acoustic problems free of characteristic wavenumbers[19]. With the aid of the CFIE, the BEFM can be applied to acoustic problems with pure Dirichlet[13] and pure Neumann[14] boundary conditions.

In this paper, a stabilized complex variable moving least-square (CVMLS) approximation[20] is used to approximate the boundary variables in the Burton-Miller formulation, a complex variable BEFM (CVBEFM) for solving the acoustic problems with arbitrary wavenumbers and mixed boundary conditions. The main work of this paper is as follows.

First, a weakly singular version of the Burton-Miller formulation is derived theoretically. The main difficulty in the numerical implementation of the Burton-Miller formulation is to calculate the hypersingular integrals[15–17]. Some regularization techniques produce integrals which are restricted to special boundary elements in BEMs or are still hard to calculate numerically. Some regularization techniques are based on the assumptions such as the solid angle is constant and/or the normal derivative of the solid angle on the boundary is zero[15–16]. In this research, by considering the normal derivative of the solid angle and using the singularity subtraction procedures for regularization, the regularization is implemented globally, rather than locally along each element as in some BEMs. Besides, the present weakly singular Burton-Miller formulation successfully gets rid of both strongly singular and hypersingular integrals and astutely avoids the computation of the solid angle and its normal derivative.

Second, a stabilized CVMLS approximation is selected to facilitate the discretization of the weakly singular Burton-Miller formulation. In the BEFM and other BIE-based meshless methods, boundary curvilinear coordinates are used to avoid the singularity in the process of boundary variable approximations, although using curvilinear coordinates is burdensome for some problems. More seriously, using curvilinear coordinates complicates the approximation of the gradients of the boundary variables. The present CVMLS approximation directly uses Cartesian coordinates, and thus facilitates the implementation of the CVBEFM and the ap-

proximation of the gradients of the boundary variables in the weakly singular Burton-Miller formulation.

Third, numerical results are provided to demonstrate the effectiveness of the current Burton-Miller CVBEFM for acoustic problems with arbitrary and large wavenumbers. The results show that the CVBEFM in conjunction with the weakly singular Burton-Miller formulation is stable and robust for all wavenumbers including the characteristic wavenumbers. In previously reported numerical results, the applications of meshless methods to acoustic problems focused mainly on $k < 10$ and seldom on $k \geqslant 100$. In this paper, although no extra term is added to eliminate the nasty pollution error existing in many numerical methods[21], the present CVBEFM can produce satisfactory results for all wavenumbers, even for extremely large wavenumbers such as $k = 10\,000$.

2 Problem description and hypersingular Burton-Miller formulation

The acoustic problem in a bounded homogeneous medium $\Omega \subset \mathbb{R}^2$ or an unbounded homogeneous medium $\Omega' = \mathbb{R}^2/(\Omega \cup \Gamma)$ is governed by the following acoustic wave equation:

$$\Delta u(\boldsymbol{x}) + k^2 u(\boldsymbol{x}) = 0, \quad \boldsymbol{x} = (x_1, x_2)^{\mathrm{T}} \in \Omega \ \text{ or } \ \Omega', \tag{1}$$

where $u(\boldsymbol{x})$ is the sound pressure, k is the wavenumber, and $\Gamma = \partial\Omega$ is the boundary of Ω. For exterior problems, u should fulfill the radiation condition at infinity as $\lim\limits_{r\to\infty} \sqrt{r}(\frac{\partial u}{\partial r} - \mathrm{i}ku) = 0$, where $r = |\boldsymbol{x}|$, and $\mathrm{i} = \sqrt{-1}$.

If the normal vector $\boldsymbol{n}_{\boldsymbol{x}}$ on the boundary Γ points from Ω into Ω' for interior problems and points from Ω' into Ω for exterior problems, the solution of both interior and exterior acoustic problems (1) can be unified as follows:

$$u(\boldsymbol{y}) = \int_\Gamma q(\boldsymbol{x}) u^*(\boldsymbol{x}, \boldsymbol{y}) \mathrm{d}\Gamma_{\boldsymbol{x}} - \int_\Gamma u(\boldsymbol{x}) \frac{\partial u^*(\boldsymbol{x}, \boldsymbol{y})}{\partial \boldsymbol{n}_{\boldsymbol{x}}} \mathrm{d}\Gamma_{\boldsymbol{x}} + u_{\mathrm{in}}(\boldsymbol{y}), \quad \boldsymbol{y} = (y_1, y_2)^{\mathrm{T}} \in \Omega \ \text{ or } \ \Omega', \tag{2}$$

while the associated singular BIE is

$$c(\boldsymbol{y}) u(\boldsymbol{y}) = \int_\Gamma q(\boldsymbol{x}) u^*(\boldsymbol{x}, \boldsymbol{y}) \mathrm{d}\Gamma_{\boldsymbol{x}} - \int_\Gamma u(\boldsymbol{x}) \frac{\partial u^*(\boldsymbol{x}, \boldsymbol{y})}{\partial \boldsymbol{n}_{\boldsymbol{x}}} \mathrm{d}\Gamma_{\boldsymbol{x}} + u_{\mathrm{in}}(\boldsymbol{y}), \quad \boldsymbol{y} \in \Gamma, \tag{3}$$

where $q(\boldsymbol{x}) = \frac{\partial u(\boldsymbol{x})}{\partial \boldsymbol{n}_{\boldsymbol{x}}}$ is the acoustical flux on $\boldsymbol{x}$, $u^*(\boldsymbol{x}, \boldsymbol{y})$ is the fundamental solution to Eq. (1), $u_{\mathrm{in}}(\boldsymbol{y})$ is the incident wave, and $c(\boldsymbol{y})$ is a coefficient determined by the boundary geometry at $\boldsymbol{y}$.

Physically, $c(\boldsymbol{y})$ denotes the solid angle in the acoustic domain[1,15–16]. Of course, we have $c(\boldsymbol{y}) = 1/2$ when Γ is smooth around $\boldsymbol{y}$. The singular BIE (3) is valid for both interior and exterior problems. However, if the normal vector $\boldsymbol{n}_{\boldsymbol{x}}$ is defined pointing from Ω into Ω' for both interior and exterior problems, it is not trivial to obtain a unified singular BIE[1,19].

Derivating the singular BIE (3) with respect to $\boldsymbol{n}_{\boldsymbol{y}}$ yields the hypersingular BIE as follows:

$$\begin{aligned} & c(\boldsymbol{y}) q(\boldsymbol{y}) + \frac{\partial c(\boldsymbol{y})}{\partial \boldsymbol{n}_{\boldsymbol{y}}} u(\boldsymbol{y}) \\ = & \int_\Gamma q(\boldsymbol{x}) \frac{\partial u^*(\boldsymbol{x}, \boldsymbol{y})}{\partial \boldsymbol{n}_{\boldsymbol{y}}} \mathrm{d}\Gamma_{\boldsymbol{x}} - \int_\Gamma u(\boldsymbol{x}) \frac{\partial^2 u^*(\boldsymbol{x}, \boldsymbol{y})}{\partial \boldsymbol{n}_{\boldsymbol{y}} \partial \boldsymbol{n}_{\boldsymbol{x}}} \mathrm{d}\Gamma_{\boldsymbol{x}} + q_{\mathrm{in}}(\boldsymbol{y}), \quad \boldsymbol{y} \in \Gamma, \end{aligned} \tag{4}$$

where $q_{\mathrm{in}}(\boldsymbol{y}) = \frac{\partial u_{\mathrm{in}}(\boldsymbol{y})}{\partial \boldsymbol{n}_{\boldsymbol{y}}}$. It should be stressed that the term $\frac{\partial c(\boldsymbol{y})}{\partial \boldsymbol{n}_{\boldsymbol{y}}} u(\boldsymbol{y})$ should appear on the right-hand side of Eq. (4), since the normal derivative $\frac{\partial c(\boldsymbol{y})}{\partial \boldsymbol{n}_{\boldsymbol{y}}}$ is usually not equal to zero when $\boldsymbol{y} \in \Gamma$[15–16].

Both the singular BIE (3) and the hypersingular BIE (4) hold for the exterior and interior acoustic problems, but their solutions may fail for the exterior problems at some characteristic wavenumbers of the associated interior problem. Since the characteristic wavenumbers of the two BIEs are different, one can use the following hypersingular Burton-Miller formulation:

$$\begin{aligned}&\alpha c(\boldsymbol{y})u(\boldsymbol{y})+\beta c(\boldsymbol{y})q(\boldsymbol{y})+\beta\frac{\partial c(\boldsymbol{y})}{\partial \boldsymbol{n}_{\boldsymbol{y}}}u(\boldsymbol{y})\\ =&\alpha\int_\Gamma q(\boldsymbol{x})u^*(\boldsymbol{x},\boldsymbol{y})\mathrm{d}\Gamma_{\boldsymbol{x}}-\alpha\int_\Gamma u(\boldsymbol{x})\frac{\partial u^*(\boldsymbol{x},\boldsymbol{y})}{\partial \boldsymbol{n}_{\boldsymbol{x}}}\mathrm{d}\Gamma_{\boldsymbol{x}}+\alpha u_{\mathrm{in}}(\boldsymbol{y})\\ &+\beta\int_\Gamma q(\boldsymbol{x})\frac{\partial u^*(\boldsymbol{x},\boldsymbol{y})}{\partial \boldsymbol{n}_{\boldsymbol{y}}}\mathrm{d}\Gamma_{\boldsymbol{x}}-\beta\int_\Gamma u(\boldsymbol{x})\frac{\partial^2 u^*(\boldsymbol{x},\boldsymbol{y})}{\partial \boldsymbol{n}_{\boldsymbol{y}}\partial \boldsymbol{n}_{\boldsymbol{x}}}\mathrm{d}\Gamma_{\boldsymbol{x}}+\beta q_{\mathrm{in}}(\boldsymbol{y}),\end{aligned}\tag{5}$$

where $\boldsymbol{y}\in\Gamma$, and α and β are coupling constants which can be taken as $\alpha=1$ and $\beta=\mathrm{i}/\max(k,1)$ to ensure the valid solutions for arbitrary wavenumbers[1,22]. Clearly, both singular and hypersingular BIEs are special cases of the hypersingular Burton-Miller formulation (5).

3 Regularization

Lemma 1 *Let $u_0^*(\boldsymbol{x},\boldsymbol{y})=-\frac{1}{2\pi}\ln|\boldsymbol{x}-\boldsymbol{y}|$. For any $\boldsymbol{y}\in\Gamma$, the solid angle $c(\boldsymbol{y})$ satisfies*

$$\int_\Gamma\frac{\partial u_0^*(\boldsymbol{x},\boldsymbol{y})}{\partial \boldsymbol{n}_{\boldsymbol{x}}}\mathrm{d}\Gamma_{\boldsymbol{x}}=-c(\boldsymbol{y}),\tag{6}$$

$$\int_\Gamma\frac{\partial^2 u_0^*(\boldsymbol{x},\boldsymbol{y})}{\partial \boldsymbol{n}_{\boldsymbol{y}}\partial \boldsymbol{n}_{\boldsymbol{x}}}\mathrm{d}\Gamma_{\boldsymbol{x}}=-\frac{\partial c(\boldsymbol{y})}{\partial \boldsymbol{n}_{\boldsymbol{y}}}.\tag{7}$$

In addition,

$$\int_\Gamma(\boldsymbol{x}-\boldsymbol{y})\frac{\partial^2 u_0^*(\boldsymbol{x},\boldsymbol{y})}{\partial \boldsymbol{n}_{\boldsymbol{y}}\partial \boldsymbol{n}_{\boldsymbol{x}}}\mathrm{d}\Gamma_{\boldsymbol{x}}=\int_\Gamma \boldsymbol{n}_{\boldsymbol{x}}\frac{\partial u_0^*(\boldsymbol{x},\boldsymbol{y})}{\partial \boldsymbol{n}_{\boldsymbol{y}}}\mathrm{d}\Gamma_{\boldsymbol{x}}+\int_\Gamma \boldsymbol{n}_{\boldsymbol{y}}\frac{\partial u_0^*(\boldsymbol{x},\boldsymbol{y})}{\partial \boldsymbol{n}_{\boldsymbol{x}}}\mathrm{d}\Gamma_{\boldsymbol{x}}.\tag{8}$$

Proof The singular BIE for the Laplace equation $\Delta v(\boldsymbol{x})=0$ is[1]

$$c(\boldsymbol{y})v(\boldsymbol{y})=\int_\Gamma\frac{\partial v(\boldsymbol{x})}{\partial \boldsymbol{n}_{\boldsymbol{x}}}u_0^*(\boldsymbol{x},\boldsymbol{y})\mathrm{d}\Gamma_{\boldsymbol{x}}-\int_\Gamma v(\boldsymbol{x})\frac{\partial u_0^*(\boldsymbol{x},\boldsymbol{y})}{\partial \boldsymbol{n}_{\boldsymbol{x}}}\mathrm{d}\Gamma_{\boldsymbol{x}},\quad \boldsymbol{y}\in\Gamma.\tag{9}$$

Setting $v(\boldsymbol{x})=1$ yields Eq. (6). Besides, since the normal derivative of a double layer potential is continuous across Γ[1], i.e.,

$$\lim_{\tilde{\boldsymbol{y}}\to\boldsymbol{y},\tilde{\boldsymbol{y}}\in\Omega}\frac{\partial}{\partial \boldsymbol{n}_{\tilde{\boldsymbol{y}}}}\int_\Gamma\frac{\partial u_0^*(\boldsymbol{x},\boldsymbol{y})}{\partial \boldsymbol{n}_{\boldsymbol{x}}}\mathrm{d}\Gamma_{\boldsymbol{x}}=\lim_{\tilde{\boldsymbol{y}}\to\boldsymbol{y},\tilde{\boldsymbol{y}}\in\Omega'}\frac{\partial}{\partial \boldsymbol{n}_{\tilde{\boldsymbol{y}}}}\int_\Gamma\frac{\partial u_0^*(\boldsymbol{x},\boldsymbol{y})}{\partial \boldsymbol{n}_{\boldsymbol{x}}}\mathrm{d}\Gamma_{\boldsymbol{x}}=\int_\Gamma\frac{\partial^2 u_0^*(\boldsymbol{x},\boldsymbol{y})}{\partial \boldsymbol{n}_{\boldsymbol{y}}\partial \boldsymbol{n}_{\boldsymbol{x}}}\mathrm{d}\Gamma_{\boldsymbol{x}},$$

using Eq. (6) yields

$$\int_\Gamma\frac{\partial^2 u_0^*(\boldsymbol{x},\boldsymbol{y})}{\partial \boldsymbol{n}_{\boldsymbol{y}}\partial \boldsymbol{n}_{\boldsymbol{x}}}\mathrm{d}\Gamma_{\boldsymbol{x}}=\frac{\partial}{\partial \boldsymbol{n}_{\boldsymbol{y}}}\int_\Gamma\frac{\partial u_0^*(\boldsymbol{x},\boldsymbol{y})}{\partial \boldsymbol{n}_{\boldsymbol{x}}}\mathrm{d}\Gamma_{\boldsymbol{x}}=-\frac{\partial c(\boldsymbol{y})}{\partial \boldsymbol{n}_{\boldsymbol{y}}},$$

which shows that Eq. (7) is true.

Taking the derivative of Eq. (9) with $\boldsymbol{n}_{\boldsymbol{y}}$ and sending $\boldsymbol{x}\to\Gamma$ yield

$$\frac{\partial c(\boldsymbol{y})}{\partial \boldsymbol{n}_{\boldsymbol{y}}}v(\boldsymbol{y})+c(\boldsymbol{y})\frac{\partial v(\boldsymbol{y})}{\partial \boldsymbol{n}_{\boldsymbol{y}}}+\int_\Gamma v(\boldsymbol{x})\frac{\partial^2 u_0^*(\boldsymbol{x},\boldsymbol{y})}{\partial \boldsymbol{n}_{\boldsymbol{y}}\partial \boldsymbol{n}_{\boldsymbol{x}}}\mathrm{d}\Gamma_{\boldsymbol{x}}=\int_\Gamma\frac{\partial v(\boldsymbol{x})}{\partial \boldsymbol{n}_{\boldsymbol{x}}}\frac{\partial u_0^*(\boldsymbol{x},\boldsymbol{y})}{\partial \boldsymbol{n}_{\boldsymbol{y}}}\mathrm{d}\Gamma_{\boldsymbol{x}}.$$

Set $v(\boldsymbol{x}) = x_i$ $(i = 1, 2)$. Then,

$$\frac{\partial c(\boldsymbol{y})}{\partial \boldsymbol{n_y}} y_i + c(\boldsymbol{y}) n_{y_i} + \int_\Gamma x_i \frac{\partial^2 u_0^*(\boldsymbol{x}, \boldsymbol{y})}{\partial \boldsymbol{n_y} \partial \boldsymbol{n_x}} \mathrm{d}\Gamma_{\boldsymbol{x}} = \int_\Gamma n_{x_i} \frac{\partial u_0^*(\boldsymbol{x}, \boldsymbol{y})}{\partial \boldsymbol{n_y}} \mathrm{d}\Gamma_{\boldsymbol{x}},$$

i.e.,

$$\frac{\partial c(\boldsymbol{y})}{\partial \boldsymbol{n_y}} \boldsymbol{y} + c(\boldsymbol{y}) \boldsymbol{n_y} + \int_\Gamma \boldsymbol{x} \frac{\partial^2 u_0^*(\boldsymbol{x}, \boldsymbol{y})}{\partial \boldsymbol{n_y} \partial \boldsymbol{n_x}} \mathrm{d}\Gamma_{\boldsymbol{x}} = \int_\Gamma \boldsymbol{n_x} \frac{\partial u_0^*(\boldsymbol{x}, \boldsymbol{y})}{\partial \boldsymbol{n_y}} \mathrm{d}\Gamma_{\boldsymbol{x}}.$$

Hence, in view of Eqs. (6) and (7), we have

$$-\boldsymbol{y} \int_\Gamma \frac{\partial^2 u_0^*(\boldsymbol{x}, \boldsymbol{y})}{\partial \boldsymbol{n_y} \partial \boldsymbol{n_x}} \mathrm{d}\Gamma_{\boldsymbol{x}} - \boldsymbol{n_y} \int_\Gamma \frac{\partial u_0^*(\boldsymbol{x}, \boldsymbol{y})}{\partial \boldsymbol{n_x}} \mathrm{d}\Gamma_{\boldsymbol{x}} + \int_\Gamma \boldsymbol{x} \frac{\partial^2 u_0^*(\boldsymbol{x}, \boldsymbol{y})}{\partial \boldsymbol{n_y} \partial \boldsymbol{n_x}} \mathrm{d}\Gamma_{\boldsymbol{x}} = \int_\Gamma \boldsymbol{n_x} \frac{\partial u_0^*(\boldsymbol{x}, \boldsymbol{y})}{\partial \boldsymbol{n_y}} \mathrm{d}\Gamma_{\boldsymbol{x}},$$

which shows that Eq. (8) is true.

Theorem 1 *The Burton-Miller formulation* (5) *can be regularized as the following weakly singular BIE*:

$$\begin{aligned}
&\alpha \int_\Gamma u(\boldsymbol{x}) \frac{\partial}{\partial \boldsymbol{n_x}} (u^*(\boldsymbol{x}, \boldsymbol{y}) - u_0^*(\boldsymbol{x}, \boldsymbol{y})) \mathrm{d}\Gamma_{\boldsymbol{x}} - \beta \int_\Gamma q(\boldsymbol{x}) \frac{\partial}{\partial \boldsymbol{n_y}} (u^*(\boldsymbol{x}, \boldsymbol{y}) - u_0^*(\boldsymbol{x}, \boldsymbol{y})) \mathrm{d}\Gamma_{\boldsymbol{x}} \\
&+ \alpha \int_\Gamma (u(\boldsymbol{x}) - u(\boldsymbol{y})) \frac{\partial u_0^*(\boldsymbol{x}, \boldsymbol{y})}{\partial \boldsymbol{n_x}} \mathrm{d}\Gamma_{\boldsymbol{x}} - \beta \int_\Gamma \nabla (u(\boldsymbol{x}) - u(\boldsymbol{y})) \cdot \boldsymbol{n_x} \frac{\partial u_0^*(\boldsymbol{x}, \boldsymbol{y})}{\partial \boldsymbol{n_y}} \mathrm{d}\Gamma_{\boldsymbol{x}} \\
&+ \beta \int_\Gamma (u(\boldsymbol{x}) - u(\boldsymbol{y}) - \nabla u(\boldsymbol{y}) \cdot (\boldsymbol{x} - \boldsymbol{y})) \frac{\partial^2 u_0^*(\boldsymbol{x}, \boldsymbol{y})}{\partial \boldsymbol{n_y} \partial \boldsymbol{n_x}} \mathrm{d}\Gamma_{\boldsymbol{x}} \\
=& \alpha \int_\Gamma q(\boldsymbol{x}) u^*(\boldsymbol{x}, \boldsymbol{y}) \mathrm{d}\Gamma_{\boldsymbol{x}} - \beta \int_\Gamma u(\boldsymbol{x}) \frac{\partial^2}{\partial \boldsymbol{n_y} \partial \boldsymbol{n_x}} (u^*(\boldsymbol{x}, \boldsymbol{y}) - u_0^*(\boldsymbol{x}, \boldsymbol{y})) \mathrm{d}\Gamma_{\boldsymbol{x}} \\
&+ \alpha u_{\mathrm{in}}(\boldsymbol{y}) + \beta q_{\mathrm{in}}(\boldsymbol{y}), \quad \boldsymbol{y} \in \Gamma. \qquad (10)
\end{aligned}$$

Proof According to Eq. (6), we have

$$\begin{aligned}
&\int_\Gamma u(\boldsymbol{x}) \frac{\partial u^*(\boldsymbol{x}, \boldsymbol{y})}{\partial \boldsymbol{n_x}} \mathrm{d}\Gamma_{\boldsymbol{x}} \\
=& \int_\Gamma u(\boldsymbol{x}) \frac{\partial}{\partial \boldsymbol{n_x}} (u^*(\boldsymbol{x}, \boldsymbol{y}) - u_0^*(\boldsymbol{x}, \boldsymbol{y})) \mathrm{d}\Gamma_{\boldsymbol{x}} + \int_\Gamma (u(\boldsymbol{x}) - u(\boldsymbol{y})) \frac{\partial u_0^*(\boldsymbol{x}, \boldsymbol{y})}{\partial \boldsymbol{n_x}} \mathrm{d}\Gamma_{\boldsymbol{x}} - c(\boldsymbol{y}) u(\boldsymbol{y}), \qquad (11) \\
&\int_\Gamma q(\boldsymbol{x}) \frac{\partial u^*(\boldsymbol{x}, \boldsymbol{y})}{\partial \boldsymbol{n_y}} \mathrm{d}\Gamma_{\boldsymbol{x}} \\
=& \int_\Gamma q(\boldsymbol{x}) \frac{\partial}{\partial \boldsymbol{n_y}} (u^*(\boldsymbol{x}, \boldsymbol{y}) - u_0^*(\boldsymbol{x}, \boldsymbol{y})) \mathrm{d}\Gamma_{\boldsymbol{x}} + \int_\Gamma \nabla u(\boldsymbol{x}) \cdot \boldsymbol{n_x} \frac{\partial u_0^*(\boldsymbol{x}, \boldsymbol{y})}{\partial \boldsymbol{n_y}} \mathrm{d}\Gamma_{\boldsymbol{x}} \\
&+ \int_\Gamma q(\boldsymbol{y}) \frac{\partial u_0^*(\boldsymbol{x}, \boldsymbol{y})}{\partial \boldsymbol{n_x}} \mathrm{d}\Gamma_{\boldsymbol{x}} + c(\boldsymbol{y}) q(\boldsymbol{y}), \qquad (12)
\end{aligned}$$

$$\begin{aligned}
&\int_\Gamma u(\boldsymbol{x})\frac{\partial^2 u^*(\boldsymbol{x},\boldsymbol{y})}{\partial \boldsymbol{n_y}\partial \boldsymbol{n_x}}\mathrm{d}\Gamma_{\boldsymbol{x}}\\
=&\int_\Gamma u(\boldsymbol{x})\frac{\partial^2}{\partial \boldsymbol{n_y}\partial \boldsymbol{n_x}}(u^*(\boldsymbol{x},\boldsymbol{y})-u_0^*(\boldsymbol{x},\boldsymbol{y}))\mathrm{d}\Gamma_{\boldsymbol{x}}\\
&+\int_\Gamma (u(\boldsymbol{x})-u(\boldsymbol{y})-\nabla u(\boldsymbol{y})\cdot(\boldsymbol{x}-\boldsymbol{y}))\frac{\partial^2 u_0^*(\boldsymbol{x},\boldsymbol{y})}{\partial \boldsymbol{n_y}\partial \boldsymbol{n_x}}\mathrm{d}\Gamma_{\boldsymbol{x}}\\
&+\nabla u(\boldsymbol{y})\cdot\int_\Gamma (\boldsymbol{x}-\boldsymbol{y})\frac{\partial^2 u_0^*(\boldsymbol{x},\boldsymbol{y})}{\partial \boldsymbol{n_y}\partial \boldsymbol{n_x}}\mathrm{d}\Gamma_{\boldsymbol{x}}+u(\boldsymbol{y})\int_\Gamma \frac{\partial^2 u_0^*(\boldsymbol{x},\boldsymbol{y})}{\partial \boldsymbol{n_y}\partial \boldsymbol{n_x}}\mathrm{d}\Gamma_{\boldsymbol{x}},
\end{aligned}\tag{13}$$

where $q(\boldsymbol{x})=\nabla u(\boldsymbol{x})\cdot\boldsymbol{n_x}$.

From Eq. (8), it follows that

$$\begin{aligned}
&\nabla u(\boldsymbol{y})\cdot\int_\Gamma (\boldsymbol{x}-\boldsymbol{y})\frac{\partial^2 u_0^*(\boldsymbol{x},\boldsymbol{y})}{\partial \boldsymbol{n_y}\partial \boldsymbol{n_x}}\mathrm{d}\Gamma_{\boldsymbol{x}}\\
=&\nabla u(\boldsymbol{y})\cdot\int_\Gamma \boldsymbol{n_x}\frac{\partial u_0^*(\boldsymbol{x},\boldsymbol{y})}{\partial \boldsymbol{n_y}}\mathrm{d}\Gamma_{\boldsymbol{x}}+\nabla u(\boldsymbol{y})\cdot\int_\Gamma \boldsymbol{n_y}\frac{\partial u_0^*(\boldsymbol{x},\boldsymbol{y})}{\partial \boldsymbol{n_x}}\mathrm{d}\Gamma_{\boldsymbol{x}}\\
=&\nabla u(\boldsymbol{y})\cdot\int_\Gamma \boldsymbol{n_x}\frac{\partial u_0^*(\boldsymbol{x},\boldsymbol{y})}{\partial \boldsymbol{n_y}}\mathrm{d}\Gamma_{\boldsymbol{x}}+q(\boldsymbol{y})\int_\Gamma \frac{\partial u_0^*(\boldsymbol{x},\boldsymbol{y})}{\partial \boldsymbol{n_x}}\mathrm{d}\Gamma_{\boldsymbol{x}}.
\end{aligned}\tag{14}$$

Inserting Eq. (14) into Eq. (13) and using Eq. (7), we have

$$\begin{aligned}
&\int_\Gamma u(\boldsymbol{x})\frac{\partial^2 u^*(\boldsymbol{x},\boldsymbol{y})}{\partial \boldsymbol{n_y}\partial \boldsymbol{n_x}}\mathrm{d}\Gamma_{\boldsymbol{x}}\\
=&\int_\Gamma u(\boldsymbol{x})\frac{\partial^2}{\partial \boldsymbol{n_y}\partial \boldsymbol{n_x}}(u^*(\boldsymbol{x},\boldsymbol{y})-u_0^*(\boldsymbol{x},\boldsymbol{y}))\mathrm{d}\Gamma_{\boldsymbol{x}}\\
&+\int_\Gamma (u(\boldsymbol{x})-u(\boldsymbol{y})-\nabla u(\boldsymbol{y})\cdot(\boldsymbol{x}-\boldsymbol{y}))\frac{\partial^2 u_0^*(\boldsymbol{x},\boldsymbol{y})}{\partial \boldsymbol{n_y}\partial \boldsymbol{n_x}}\mathrm{d}\Gamma_{\boldsymbol{x}}\\
&+\int_\Gamma \nabla u(\boldsymbol{y})\cdot\boldsymbol{n_x}\frac{\partial u_0^*(\boldsymbol{x},\boldsymbol{y})}{\partial \boldsymbol{n_y}}\mathrm{d}\Gamma_{\boldsymbol{x}}+q(\boldsymbol{y})\int_\Gamma \frac{\partial u_0^*(\boldsymbol{x},\boldsymbol{y})}{\partial \boldsymbol{n_x}}\mathrm{d}\Gamma_{\boldsymbol{x}}-u(\boldsymbol{y})\frac{\partial c(\boldsymbol{y})}{\partial \boldsymbol{n_y}}.
\end{aligned}\tag{15}$$

Finally, substituting Eqs. (11), (12), and (15) into Eq. (5) yields the desired result.

Remark 1 Let $r=|\boldsymbol{x}-\boldsymbol{y}|$. Then,

$$u^*(\boldsymbol{x},\boldsymbol{y})=\frac{\mathrm{i}}{4}H_0^{(1)}(kr),\quad \frac{\partial u^*(\boldsymbol{x},\boldsymbol{y})}{\partial \boldsymbol{n_x}}=-\frac{\mathrm{i}k}{4}H_1^{(1)}(kr)\frac{\partial r}{\partial \boldsymbol{n_x}},\tag{16}$$

$$\frac{\partial^2 u^*(\boldsymbol{x},\boldsymbol{y})}{\partial \boldsymbol{n_y}\partial \boldsymbol{n_x}}=\mathrm{i}k\Big(\frac{1}{2r}H_1^{(1)}(kr)-\frac{k}{4}H_0^{(1)}(kr)\Big)\frac{\partial r}{\partial \boldsymbol{n_x}}\frac{\partial r}{\partial \boldsymbol{n_y}}+\frac{\mathrm{i}k}{4r}H_1^{(1)}(kr)\boldsymbol{n_x}\cdot\boldsymbol{n_y},\tag{17}$$

where $H_0^{(1)}$ and $H_1^{(1)}$ are the first kind Hankel functions of orders zero and one, respectively. When $r=|\boldsymbol{x}-\boldsymbol{y}|\to 0$, we have

$$\begin{aligned}
&\frac{\partial}{\partial \boldsymbol{n_x}}(u^*(\boldsymbol{x},\boldsymbol{y})-u_0^*(\boldsymbol{x},\boldsymbol{y}))\sim\mathcal{O}(1),\quad \frac{\partial}{\partial \boldsymbol{n_y}}(u^*(\boldsymbol{x},\boldsymbol{y})-u_0^*(\boldsymbol{x},\boldsymbol{y}))\sim\mathcal{O}(1),\\
&u(\boldsymbol{x})-u(\boldsymbol{y})\sim\mathcal{O}(r),\quad \frac{\partial u_0^*(\boldsymbol{x},\boldsymbol{y})}{\partial \boldsymbol{n_x}}\sim\mathcal{O}\Big(\frac{1}{r}\Big),\\
&\nabla(u(\boldsymbol{x})-u(\boldsymbol{y}))\cdot\boldsymbol{n_x}\sim\mathcal{O}(r),\quad \frac{\partial u_0^*(\boldsymbol{x},\boldsymbol{y})}{\partial \boldsymbol{n_y}}\sim\mathcal{O}\Big(\frac{1}{r}\Big),
\end{aligned}$$

$$u(\boldsymbol{x})-u(\boldsymbol{y})-\nabla u(\boldsymbol{y})\cdot(\boldsymbol{x}-\boldsymbol{y})\sim\mathcal{O}(r^2),\quad \frac{\partial^2 u_0^*(\boldsymbol{x},\boldsymbol{y})}{\partial \boldsymbol{n}_{\boldsymbol{y}}\partial \boldsymbol{n}_{\boldsymbol{x}}}\sim\mathcal{O}\Big(\frac{1}{r^2}\Big).$$

Thus, as $\boldsymbol{x}\to\boldsymbol{y}$, i.e., $r\to 0$, the singularities in all integrals on the left-hand side of Eq. (10) can be canceled completely. As a result, all integrals on the left-hand side of Eq. (10) are always regular.

Remark 2 Let $c=0.577\,215\,664\,9\cdots$ be the Euler constant. As $r=|\boldsymbol{x}-\boldsymbol{y}|\to 0$, $u^*(\boldsymbol{x},\boldsymbol{y})$ can be expanded as[19]

$$u^*(\boldsymbol{x},\boldsymbol{y})=-\frac{1}{2\pi}\ln\frac{kr}{2}+\frac{\mathrm{i}}{4}-\frac{c}{2\pi}+\frac{\mathrm{i}}{4}\sum_{m=1}^{\infty}\frac{(-1)^m}{(m!)^2}\Big(\frac{kr}{2}\Big)^{2m}\Big(1+\frac{2\mathrm{i}}{\pi}\Big(\ln\frac{kr}{2}+c-\sum_{j=1}^{m}\frac{1}{j}\Big)\Big),$$

from which it can be verified that

$$u^*(\boldsymbol{x},\boldsymbol{y})\sim\mathcal{O}(\ln r),\quad \frac{\partial^2}{\partial \boldsymbol{n}_{\boldsymbol{y}}\partial \boldsymbol{n}_{\boldsymbol{x}}}(u^*(\boldsymbol{x},\boldsymbol{y})-u_0^*(\boldsymbol{x},\boldsymbol{y}))\sim\mathcal{O}(\ln r).$$

Thus, the two integrals on the right-hand side of Eq. (10) have weak logarithmic singularities as $\boldsymbol{x}\to\boldsymbol{y}$.

Remark 3 Equation (10) is the weakly singular version of the hypersingular Burton-Miller formulation (5). Undoubtedly, similar to Eq. (5), Eq. (10) admits a unique solution for all wavenumbers. However, compared with Eq. (5), Eq. (10) gets rid of both strongly singular and hypersingular integrals.

Remark 4 Equation (10) is valid for both interior and exterior acoustic problems with mixed boundary conditions of Dirichlet and Neumann types. When $\alpha=1$ and $\beta=0$, Eq. (10) is degradated as the weakly singular form of the singular BIE (3). When $\alpha=0$ and $\beta=1$, Eq. (10) is the weakly singular form of the hypersingular BIE (4). Furthermore, by setting $k=0$ in Eq. (10), we can obtain the weakly singular forms of the singular and hypersingular BIEs for Laplace problems.

Remark 5 The solid angle $c(\boldsymbol{y})$ and its normal derivative $\frac{\partial c(\boldsymbol{y})}{\partial \boldsymbol{n}_{\boldsymbol{y}}}$ are not included in Eq. (10). Compared with Eq. (5), the present weakly singular Burton-Miller formulation does not need the terms $c(\boldsymbol{y})$ and $\frac{\partial c(\boldsymbol{y})}{\partial \boldsymbol{n}_{\boldsymbol{y}}}$, and thus astutely avoids the computation of the two terms. In previous studies, it was usually assumed that $c(\boldsymbol{y})\equiv 1/2$ and/or $\frac{\partial c(\boldsymbol{y})}{\partial \boldsymbol{n}_{\boldsymbol{y}}}\equiv 0$. Such assumptions are not required in the present formulation (10).

4 Meshless discretization

4.1 Boundary variable approximations

To solve the weakly singular Burton-Miller formulation (10) numerically, let $\{\boldsymbol{x}_I\}_{I=1}^N$ be N nodes on the boundary Γ and $h=\max\limits_{1\leqslant I\leqslant N}\min\limits_{1\leqslant J\leqslant N,J\neq I}|\boldsymbol{x}_I-\boldsymbol{x}_J|$ be the nodal spacing. Using complex variables, the point $\boldsymbol{x}=(x_1,x_2)^{\mathrm{T}}\in\Gamma$ and the node $\boldsymbol{x}_I=(x_{I1},x_{I2})^{\mathrm{T}}\in\Gamma$ can be denoted as $z=x_1+\mathrm{i}x_2$ and $z_I=x_{I1}+\mathrm{i}x_{I2}$, respectively.

To obtain the meshless approximation of the boundary function $u(z)$, we define

$$u(z,z^*)=\sum_{j=0}^{m}\overline{p}_j(z^*)a_j(z),\quad\forall z\in\Gamma,\tag{18}$$

where z^* can either be z or a node z_I in the influence domain of z, $a_j(z)$ is the coefficient, and $\overline{p}_j(z)$ is the conjugate of the basis function $p_j(z)$. As proven in Refs. [20] and [23], the

shifted and scaled function $p_j(z)=(z-z^e)^j/h^j$ can enhance the stability and performance of the CVMLS approximation, where z^e is fixed in the influence domain of z. Minimizing

$$\sum_{I\in\wedge(z)} w_I(z)\Big|\sum_{j=0}^{m}\overline{p}_j(z_I)a_j(z)-\widehat{u}_I\Big|^2$$

yields

$$a_j(z)=(\boldsymbol{A}^{-1}(z)\boldsymbol{B}(z)\widehat{\boldsymbol{u}})_j, \tag{19}$$

where $\widehat{u}_I$ is the approximation to the nodal value $u(z_I)$, the set $\wedge(z)\triangleq\{I_1,I_2,\cdots,I_\tau\}\subseteq\{1,2,\cdots,N\}$ is defined such that $I\in\wedge(z)$ if and only if the weight function $w_I(z)>0$, $\widehat{\boldsymbol{u}}=(\widehat{u}_{I_1},\widehat{u}_{I_2},\cdots,\widehat{u}_{I_\tau})^{\mathrm{T}}$, $\boldsymbol{A}_{kj}(z)=\sum\limits_{I\in\wedge(z)} w_I(z)\overline{p}_k(z_I)p_j(z_I)$ for $k,j=0,1,\cdots,m$, and $\boldsymbol{B}_{j\ell}(z)=w_{I_\ell}(z)p_j(z_{I_\ell})$ for $j=0,1,\cdots,m$ and $\ell=1,2,\cdots\tau$. Inserting Eq. (19) into Eq. (18) yields the CVMLS approximation of $u(z)$ as follows:

$$u(z)=u(z,z^*)\,|_{z^*=z}=\sum_{I=1}^{N}\Phi_I(z)\widehat{u}_I, \tag{20}$$

where the CVMLS shape function is

$$\Phi_I(z)=\begin{cases}\displaystyle\sum_{j=0}^{m}\overline{p}_j(z)(\boldsymbol{A}^{-1}(z)\boldsymbol{B}(z))_{jk}, & I=I_k\in\wedge(z),\\ 0, & I\notin\wedge(z).\end{cases} \tag{21}$$

Similarly, the CVMLS approximation of the boundary function $q(z)$ is

$$q(z)=\sum_{I=1}^{N}\Phi_I(z)\widehat{q}_I, \tag{22}$$

where $\widehat{q}_I$ is the approximation to the nodal value $q(z_I)$.

4.2 Discretization for mixed boundary conditions

Using Eqs. (20) and (22), the weakly singular Burton-Miller formulation (10) can be discretized as the following linear system of algebraic equations:

$$\begin{aligned}
&\alpha\sum_{I=1}^{N}\widehat{u}_I\int_\Gamma\Phi_I(\boldsymbol{x})\frac{\partial}{\partial\boldsymbol{n}_{\boldsymbol{x}}}(u^*(\boldsymbol{x},\boldsymbol{x}_j)-u_0^*(\boldsymbol{x},\boldsymbol{x}_j))\mathrm{d}\Gamma_{\boldsymbol{x}}\\
&-\beta\sum_{I=1}^{N}\widehat{q}_I\int_\Gamma\Phi_I(\boldsymbol{x})\frac{\partial}{\partial\boldsymbol{n}_{\boldsymbol{x}_j}}(u^*(\boldsymbol{x},\boldsymbol{x}_j)-u_0^*(\boldsymbol{x},\boldsymbol{x}_j))\mathrm{d}\Gamma_{\boldsymbol{x}}\\
&+\alpha\sum_{I=1}^{N}\widehat{u}_I\int_\Gamma(\Phi_I(\boldsymbol{x})-\Phi_I(\boldsymbol{x}_j))\frac{\partial u_0^*(\boldsymbol{x},\boldsymbol{x}_j)}{\partial\boldsymbol{n}_{\boldsymbol{x}}}\mathrm{d}\Gamma_{\boldsymbol{x}}\\
&-\beta\sum_{I=1}^{N}\widehat{u}_I\int_\Gamma\nabla(\Phi_I(\boldsymbol{x})-\Phi_I(\boldsymbol{x}_j))\cdot\boldsymbol{n}_{\boldsymbol{x}}\frac{\partial u_0^*(\boldsymbol{x},\boldsymbol{x}_j)}{\partial\boldsymbol{n}_{\boldsymbol{x}_j}}\mathrm{d}\Gamma_{\boldsymbol{x}}\\
&+\beta\sum_{I=1}^{N}\widehat{u}_I\int_\Gamma(\Phi_I(\boldsymbol{x})-\Phi_I(\boldsymbol{x}_j)-\nabla\Phi_I(\boldsymbol{x}_j)\cdot(\boldsymbol{x}-\boldsymbol{x}_j))\frac{\partial^2u_0^*(\boldsymbol{x},\boldsymbol{x}_j)}{\partial\boldsymbol{n}_{\boldsymbol{x}_j}\partial\boldsymbol{n}_{\boldsymbol{x}}}\mathrm{d}\Gamma_{\boldsymbol{x}}
\end{aligned}$$

$$= \alpha \sum_{I=1}^{N} \widehat{q}_I \int_\Gamma \Phi_I(\boldsymbol{x}) u^*(\boldsymbol{x}, \boldsymbol{x}_j) \mathrm{d}\Gamma_{\boldsymbol{x}} - \beta \sum_{I=1}^{N} \widehat{u}_I \int_\Gamma \Phi_I(\boldsymbol{x}) \frac{\partial^2}{\partial \boldsymbol{n}_{\boldsymbol{x}_j} \partial \boldsymbol{n}_{\boldsymbol{x}}} (u^*(\boldsymbol{x}, \boldsymbol{x}_j) - u_0^*(\boldsymbol{x}, \boldsymbol{x}_j)) \mathrm{d}\Gamma_{\boldsymbol{x}}$$
$$+ \alpha u_{\mathrm{in}}(\boldsymbol{x}_j) + \beta q_{\mathrm{in}}(\boldsymbol{x}_j), \quad j = 1, 2, \cdots, N. \tag{23}$$

All integrals on the left-hand side of Eq. (23) are always regular and can be calculated by using the standard Gaussian quadrature. The integrals on the right-hand side of Eq. (23) contain weak logarithmic singularities and can be calculated by the logarithmical Gaussian quadrature or the improved integration procedure[19].

Since the CVMLS shape function $\Phi_j(\boldsymbol{x})$ lacks the delta function property[18,20], i.e., $\Phi_j(\boldsymbol{x}_I) \neq \delta_{jI}$, we have $\widehat{u}_I \neq u(\boldsymbol{x}_I)$ and $\widehat{q}_I \neq q(\boldsymbol{x}_I)$. Thus, as in other meshless methods[24–28], the boundary conditions in the present CVBEFM must be dealt with carefully. For problems in potential theory and linear elasticity, the boundary conditions in the boundary node method can be satisfied by coupling discretized BIEs in terms of approximate nodal variables, together with equations relating these approximations to their exact values through the MLS approximation[18]. For acoustic problems, an analogous technique is adopted in this study.

The mixed boundary conditions for the acoustic wave equation (1) are

$$u(\boldsymbol{x}) = \overline{u}(\boldsymbol{x}), \quad \boldsymbol{x} \in \Gamma_u, \tag{24}$$
$$q(\boldsymbol{x}) = \overline{q}(\boldsymbol{x}), \quad \boldsymbol{x} \in \Gamma_q = \Gamma / \Gamma_u, \tag{25}$$

where $\overline{u}$ and $\overline{q}$ are known. In this case, the unknown boundary data are q on Γ_u and u on Γ_q.

To simplify the representation, we assume that the first N_u boundary nodes $\{\boldsymbol{x}_j\}_{j=1}^{N_u} \subset \Gamma_u$ and the remaining $N - N_u$ boundary nodes $\{\boldsymbol{x}_j\}_{j=N_u+1}^{N} \subset \Gamma_q$. For a well-posed problem, the values of either $u(\boldsymbol{x}_j)$ or $q(\boldsymbol{x}_j)$ are known at each node $\boldsymbol{x}_j$. Then, inserting Eq. (20) into Eq. (24) and collocating Eq. (24) for the boundary nodes $\{\boldsymbol{x}_j\}_{j=1}^{N_u} \subset \Gamma_u$ yield

$$\sum_{I=1}^{N} \Phi_I(\boldsymbol{x}_j) \widehat{u}_I = \overline{u}(\boldsymbol{x}_j), \quad j = 1, 2, \cdots, N_u. \tag{26}$$

Besides, inserting Eq. (22) into Eq. (25) and collocating Eq. (25) for the nodes $\{\boldsymbol{x}_j\}_{j=N_u+1}^{N} \subset \Gamma_q$ yield

$$\sum_{I=1}^{N} \Phi_I(\boldsymbol{x}_j) \widehat{q}_I = \overline{q}(\boldsymbol{x}_j), \quad j = N_u + 1, N_u + 2, \cdots, N. \tag{27}$$

Equations (23), (26), and (27) form a linear system of $2N$ algebraic equations, and can be solved together for the $2N$ unknowns $\{\widehat{u}_I\}_{I=1}^{N}$ and $\{\widehat{q}_I\}_{I=1}^{N}$. Finally, the pressure u in the acoustic medium can be approximated by using Eq. (2) as follows:

$$u_h(\boldsymbol{y}) = \sum_{I=1}^{N} \widehat{q}_I \int_\Gamma \Phi_I(\boldsymbol{x}) u^*(\boldsymbol{x}, \boldsymbol{y}) \mathrm{d}\Gamma_{\boldsymbol{x}} - \sum_{I=1}^{N} \widehat{u}_I \int_\Gamma \Phi_I(\boldsymbol{x}) \frac{\partial u^*(\boldsymbol{x}, \boldsymbol{y})}{\partial \boldsymbol{n}_{\boldsymbol{x}}} \mathrm{d}\Gamma_{\boldsymbol{x}} + u_{\mathrm{in}}(\boldsymbol{y}), \quad \boldsymbol{y} \in \Omega \text{ or } \Omega'.$$

4.3 Discretization for pure Dirichlet or Neumann boundary conditions

The procedure in Subsection 4.2 is valid for mixed boundary conditions including pure Dirichlet or Neumann types. This procedure makes that the number of algebraic equations is $2N$ and the unknowns comprise both $\widehat{u}_I$ and $\widehat{q}_I$ for all boundary nodes $\{\boldsymbol{x}_I\}_{I=1}^{N} \subset \Gamma$. In the cases of pure Dirichlet boundary condition (i.e., $\Gamma_q = \varnothing$) or pure Neumann boundary condition (i.e., $\Gamma_u = \varnothing$), the number of algebraic equations can be reduced into N. In this section, the

detailed formulation is presented for pure Dirichlet boundary condition. The corresponding formulation for pure Neumann boundary condition is similar.

For Eq. (1), if the given boundary condition is pure Dirichlet type, i.e.,

$$u(\boldsymbol{x}) = \overline{u}(\boldsymbol{x}), \quad \boldsymbol{x} \in \Gamma, \tag{28}$$

the unknown function is just the acoustical flux q on Γ. In this case, since u is known on Γ, the approximation for u in Eq. (20) is no longer required. Thus, with Eq. (22) only, the weakly singular Burton-Miller formulation (10) can be discretized as follows:

$$\begin{aligned}
&\beta_1 \int_\Gamma \overline{u}(\boldsymbol{x}) \frac{\partial}{\partial \boldsymbol{n}_{\boldsymbol{x}}} (u^*(\boldsymbol{x}, \boldsymbol{x}_j) - u_0^*(\boldsymbol{x}, \boldsymbol{x}_j)) \mathrm{d}\Gamma_{\boldsymbol{x}} \\
&- \beta_2 \sum_{I=1}^{N} \widehat{q}_I \int_\Gamma \Phi_I(\boldsymbol{x}) \frac{\partial}{\partial \boldsymbol{n}_{\boldsymbol{x}_j}} (u^*(\boldsymbol{x}, \boldsymbol{x}_j) - u_0^*(\boldsymbol{x}, \boldsymbol{x}_j)) \mathrm{d}\Gamma_{\boldsymbol{x}} \\
&+ \beta_1 \int_\Gamma (\overline{u}(\boldsymbol{x}) - \overline{u}(\boldsymbol{x}_j)) \frac{\partial u_0^*(\boldsymbol{x}, \boldsymbol{x}_j)}{\partial \boldsymbol{n}_{\boldsymbol{x}}} \mathrm{d}\Gamma_{\boldsymbol{x}} - \beta_2 \int_\Gamma \nabla(\overline{u}(\boldsymbol{x}) - \overline{u}(\boldsymbol{x}_j)) \cdot \boldsymbol{n}_{\boldsymbol{x}} \frac{\partial u_0^*(\boldsymbol{x}, \boldsymbol{x}_j)}{\partial \boldsymbol{n}_{\boldsymbol{x}_j}} \mathrm{d}\Gamma_{\boldsymbol{x}} \\
&+ \beta_2 \int_\Gamma (\overline{u}(\boldsymbol{x}) - \overline{u}(\boldsymbol{x}_j) - \nabla \overline{u}(\boldsymbol{x}_j) \cdot (\boldsymbol{x} - \boldsymbol{x}_j)) \frac{\partial^2 u_0^*(\boldsymbol{x}, \boldsymbol{x}_j)}{\partial \boldsymbol{n}_{\boldsymbol{x}_j} \partial \boldsymbol{n}_{\boldsymbol{x}}} \mathrm{d}\Gamma_{\boldsymbol{x}} \\
&= \beta_1 \sum_{I=1}^{N} \widehat{q}_I \int_\Gamma \Phi_I(\boldsymbol{x}) u^*(\boldsymbol{x}, \boldsymbol{x}_j) \mathrm{d}\Gamma_{\boldsymbol{x}} - \beta_2 \int_\Gamma \overline{u}(\boldsymbol{x}) \frac{\partial^2}{\partial \boldsymbol{n}_{\boldsymbol{x}_j} \partial \boldsymbol{n}_{\boldsymbol{x}}} (u^*(\boldsymbol{x}, \boldsymbol{x}_j) - u_0^*(\boldsymbol{x}, \boldsymbol{x}_j)) \mathrm{d}\Gamma_{\boldsymbol{x}} \\
&+ \beta_1 u_{\mathrm{in}}(\boldsymbol{x}_j) + \beta_2 q_{\mathrm{in}}(\boldsymbol{x}_j), \quad j = 1, 2, \cdots, N,
\end{aligned}$$

which can be solved directly to obtain the N unknowns $\{\widehat{q}_I\}_{I=1}^N$. Finally, the pressure u in the acoustic medium can be approximated as follows:

$$u_h(\boldsymbol{y}) = \sum_{I=1}^{N} \widehat{q}_I \int_\Gamma \Phi_I(\boldsymbol{x}) u^*(\boldsymbol{x}, \boldsymbol{y}) \mathrm{d}\Gamma_{\boldsymbol{x}} - \int_\Gamma \overline{u}(\boldsymbol{x}) \frac{\partial u^*(\boldsymbol{x}, \boldsymbol{y})}{\partial \boldsymbol{n}_{\boldsymbol{x}}} \mathrm{d}\Gamma_{\boldsymbol{x}} + u_{\mathrm{in}}(\boldsymbol{y}), \quad \boldsymbol{y} \in \Omega \text{ or } \Omega'.$$

5 Numerical examples

Three examples are solved in this section to show the efficiency of the present Burton-Miller CVBEFM. In this study, the quadratic basis function is used, and the radius of the influence domain for meshfree approximation is $2.5h$. To evaluate the performance of the method, we define an average relative error as follows:

$$e(u) = \frac{1}{N_t} \sum_{j=1}^{N_t} \left| \frac{u(\boldsymbol{x}_j) - u_h(\boldsymbol{x}_j)}{u(\boldsymbol{x}_j)} \right|,$$

where $u(\boldsymbol{x}_j)$ and $u_h(\boldsymbol{x}_j)$ are analytical and numerical results of $u(\boldsymbol{x})$ on the N_t points $\boldsymbol{x}_j$, respectively.

5.1 Example 1

The first example solves an exterior acoustic problem in an infinitely long cylinder with the radius $a = 2.0$. In the polar coordinate system (r, θ), the Neumann boundary condition is imposed as $\frac{\partial u}{\partial \boldsymbol{n}} = \mathrm{e}^{\mathrm{i}\theta}$, and the analytical solution is[29]

$$u(r, \theta) = \frac{a \mathrm{e}^{\mathrm{i}\theta} H_1^{(1)}(kr)}{H_1^{(1)}(ak) - ak H_0^{(1)}(ak)}, \quad r \geqslant a, \quad 0 \leqslant \theta < 2\pi. \tag{29}$$

To study the performance of the CVBEFM for all wavenumbers, the weakly singular versions of the singular BIE (i.e., $\alpha = 1$ and $\beta = 0$ in Eq. (10)), the hypersingular BIE (i.e., $\alpha = 0$ and $\beta = 1$ in Eq. (10)), and the Burton-Miller formulation (10) are independently used in the CVBEFM. Figure 1 depicts the results of $|u(r, \theta)|$ at $(4.0, \pi/4)$ with respect to the wavenumber k obtained by using 20 boundary nodes, Fig. 2 depicts the error $e(u)$, while Fig. 3 depicts the condition number of the system matrices.

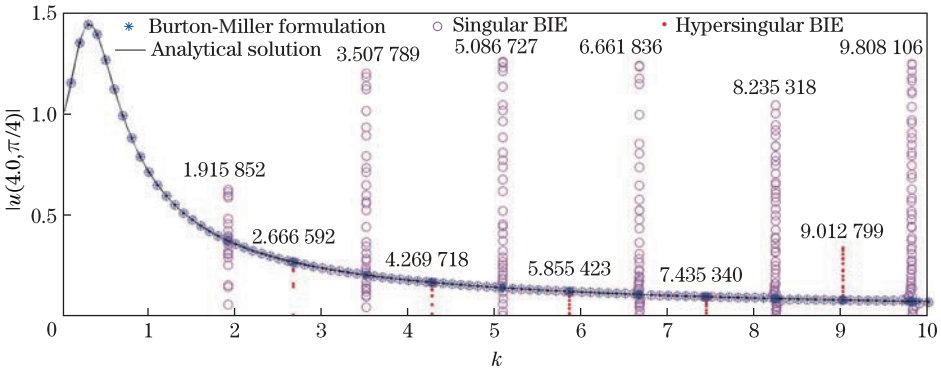

Fig. 1 Results of $|u(4.0, \pi/4)|$ versus k obtained by the CVBEFM with three BIEs (color online)

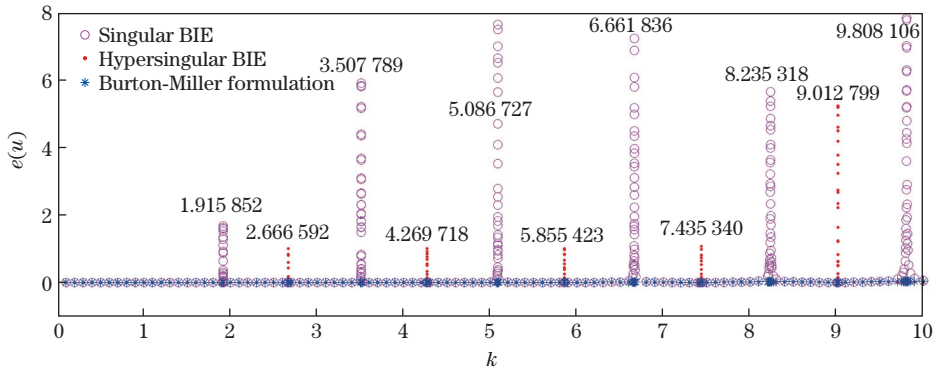

Fig. 2 Results of $e(u)$ versus k obtained by the CVBEFM with three BIEs (color online)

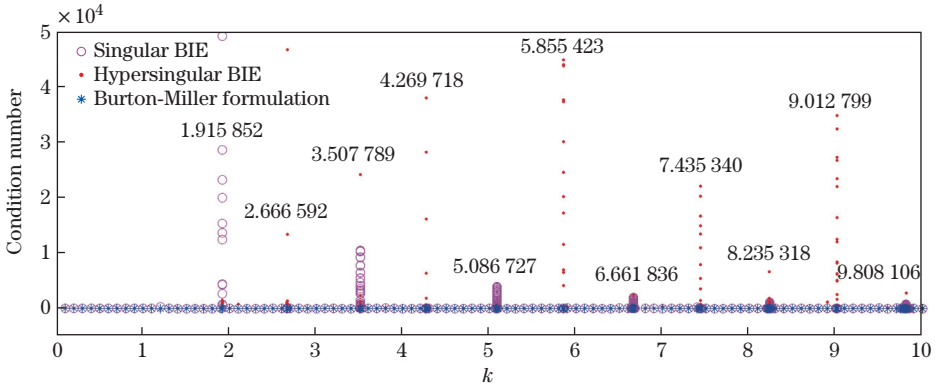

Fig. 3 Results of the condition number versus k obtained by the CVBEFM with three BIEs (color online)

From Figs. 1 and 2, we can find that the singular BIE performs worse as k approximates to 1.915 852, 3.507 789, 5.086 727, 6.661 836, 8.235 318, and 9.808 106, the hypersingular BIE

performs worse as k approximates to 2.666 592, 4.269 718, 5.855 423, 7.435 340, and 9.012 799, while the Burton-Miller formulation produces satisfactory results in all cases. Additionally, from Fig. 3, we can find that singular and hypersingular BIEs may produce large condition numbers when k approximates to these characteristic wavenumbers, but the Burton-Miller formulation produces well-conditioned system matrices in all cases. Consequently, the CVBEFM in conjunction with the Burton-Miller formulation is robust to avoid the influence of characteristic wavenumbers.

In Fig. 4, the convergence of the Burton-Miller CVBEFM is displayed for $k = 1$, 1.915 852, 2.666 592, 3.507 789, 4.269 718, 5.086 727, 5.855 423, 6.661 836, 7.435 34, 8.235 318, 9.012 799, 9.808 106, and 10. As shown in the figure, the average related error $e(u)$ decreases monotonously and quickly when the nodal spacing h decreases. Thus, the Burton-Miller CVBEFM is able to produce stable convergence results with high experimental convergence rate, about 3 even for characteristic wavenumbers. However, the accuracy does not change monotonously when the wavenumber increases. The reason is unclear and requires further research.

In Fig. 5, the absolute error $|u - u_h|$ at $(r, \theta) = (4.0, \pi/4)$ of the Burton-Miller CVBEFM obtained by using 128 boundary nodes is displayed for some wavenumbers. The results of the BEM[29] obtained by using 128 boundary elements and the BPIM[3] obtained by using 128 boundary nodes are also displayed for comparison. We can find that the precision of the CVBEFM is higher than the precision of either the BEM or the BPIM. Especially, the precision of the CVBEFM is several orders of magnitude higher than that of the BEM.

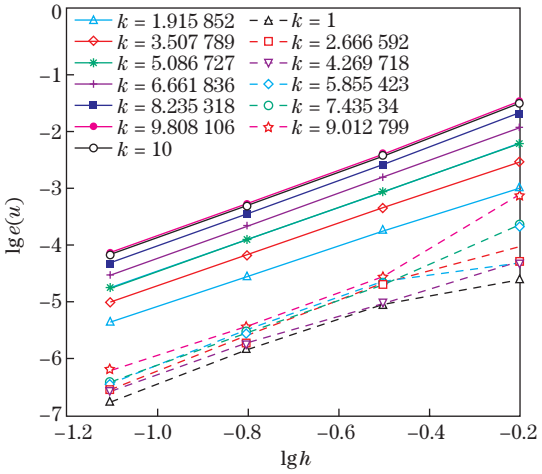

Fig. 4 Results of $e(u)$ at different k for the first example (color online)

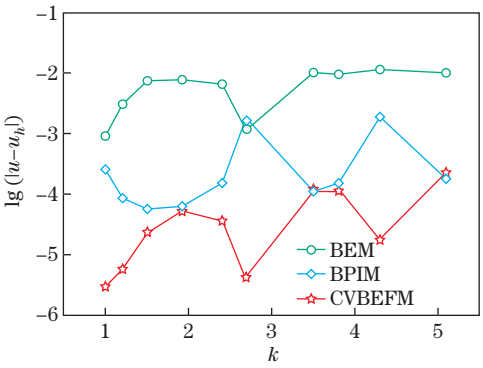

Fig. 5 Results of $|u - u_h|$ at $(r, \theta) = (4.0, \pi/4)$ obtained by the BEM, the BPIM, and the CVBEFM (color online)

It is well-known that the solutions of acoustic problems are highly oscillatory for large wavenumbers. Then, because of the nasty pollution error, in many numerical techniques, the node number must increase much faster than the wavenumber so as to obtain satisfactory numerical results[21]. To study the performance of the Burton-Miller CVBEFM for extremely large wavenumbers, Fig. 6 compares the analytical and numerical results of the real part of $u(r, \pi/4)$ for $r \in [2.0, 2.1]$ and $k = 2\,500$, while Fig. 7 depicts the absolute error $|u - u_h|$ of $u(r, \pi/4)$ for $r \in [2.0, 3.0]$. These numerical results are obtained by using $k = 2\,500$, $N = 2\,500$, and $a = 1.0$. Although the solution is highly oscillatory for this large wavenumber, Figs. 6 and 7 show that the Burton-Miller CVBEFM produces very accurate numerical results.

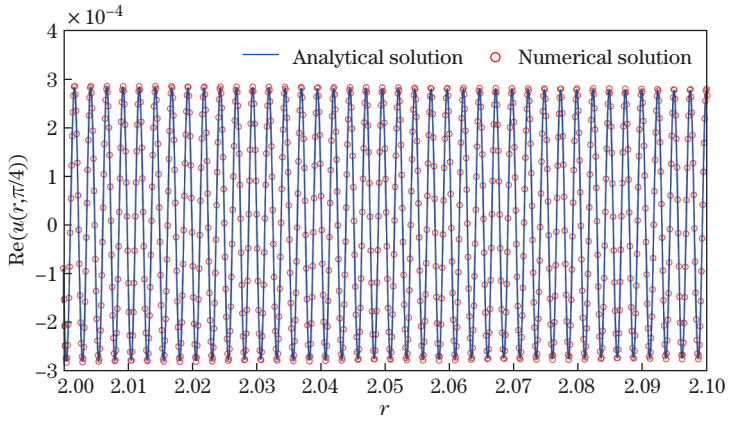

Fig. 6 Real part of $u(r, \pi/4)$, where $k = 2\,500$ and $N = 2\,500$ (color online)

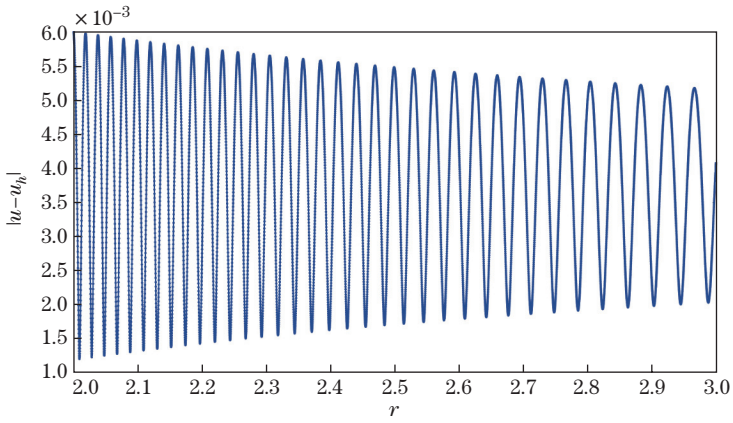

Fig. 7 Results of $|u - u_h|$ of $u(r, \pi/4)$, where $k = 2\,500$ and $N = 2\,500$ (color online)

In Table 1, the relative error $|u - u_h|/|u|$ at four points and the average relative error $e(u)$ of the Burton-Miller CVBEFM are displayed for various wavenumbers k. Although the number of boundary nodes is set to be $N = k$ in this analysis, from Table 1, we can find that the present CVBEFM can produce satisfactory results, even for extremely large wavenumbers such as $k = 10\,000$.

Table 1 Errors of the CVBEFM obtained by using various k with $N = k$

Error	Point	k							
		50	100	250	500	1 000	2 500	5 000	10 000
$\|u - u_h\|/\|u\|$	$(2.0, \pi/4)$	0.015 8	0.007 6	0.018 9	0.035 5	0.042 8	0.006 0	0.027 0	0.047 5
	$(2.0, 5\pi/8)$	0.020 2	0.011 1	0.019 3	0.040 5	0.038 6	0.001 0	0.032 3	0.047 5
	$(2.0, 7\pi/6)$	0.015 4	0.010 1	0.019 3	0.033 7	0.042 7	0.001 5	0.034 9	0.047 7
	$(2.0, 11\pi/6)$	0.018 9	0.006 9	0.019 2	0.039 1	0.036 6	0.008 3	0.027 2	0.056 1
$e(u)$	–	0.017 9	0.009 8	0.018 9	0.037 4	0.040 9	0.003 8	0.029 8	0.050 6

5.2 Example 2

The second example solves an exterior acoustic problem describing an incident plane wave $u_{\text{in}}(r, \theta) = \mathrm{e}^{\mathrm{i}kr\cos\theta}$ scattered by an infinitely long cylinder with the radius $a = 2.0$. The

Dirichlet boundary condition is imposed for the scattered wave field u_{s} as $u_{\mathrm{s}} = 0$, and the analytical solution is[30]

$$u_{\mathrm{s}}(r,\theta) = -\frac{\mathrm{J}_0(ka)}{H_0^{(1)}(ka)} H_0^{(1)}(kr) - 2\sum_{t=1}^{\infty} \mathrm{i}^t \frac{\mathrm{J}_t(ka)}{H_t^{(1)}(ka)} H_t^{(1)}(kr)\cos(t\theta),$$

where $r \geqslant a$, $0 \leqslant \theta < 2\pi$, J_t is the Bessel function of order t, and $H_t^{(1)}$ is the Hankel function of the first kind of order t. The total wave field for this example is $u = u_{\mathrm{s}} + u_{\mathrm{in}}$.

Figure 8 shows the distributions of the scattered wave field u_{s} and the associated absolute error $|u_{\mathrm{s}} - u_{\mathrm{sh}}|$ obtained by the Burton-Miller CVBEFM with 200 boundary nodes for $k = 5\pi$. We can find that the error is less than 7×10^{-3}, which indicates that the present CVBEFM obtains very efficient results.

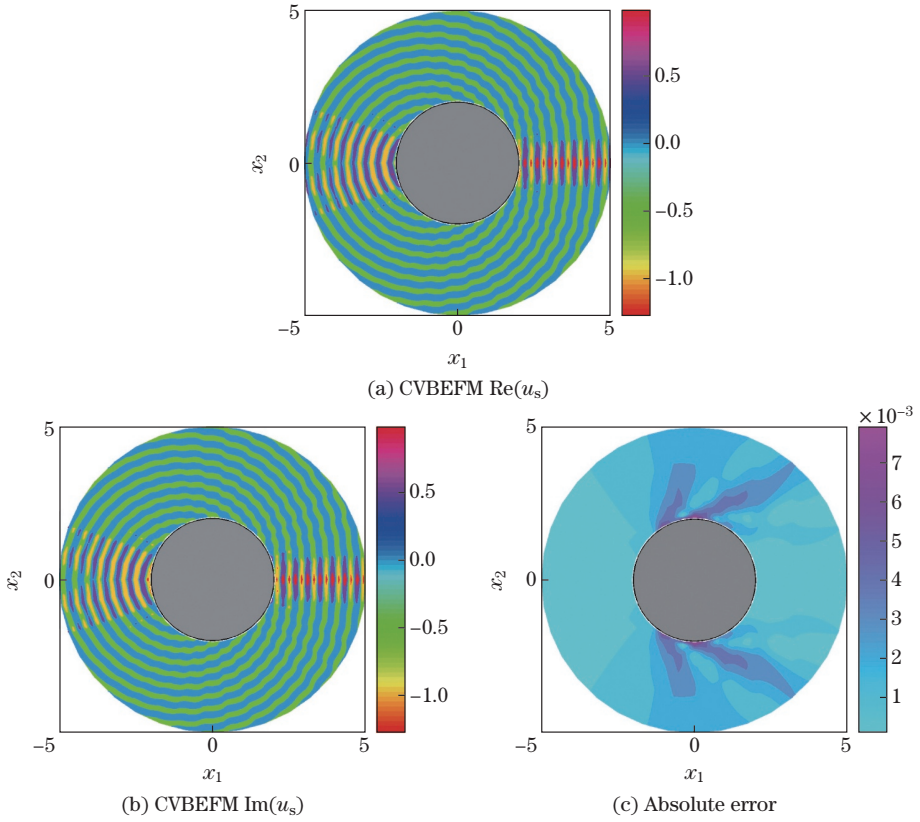

(a) CVBEFM Re(u_{s})

(b) CVBEFM Im(u_{s})

(c) Absolute error

Fig. 8 Real and imaginary parts of u_{s} and $|u_{\mathrm{s}} - u_{\mathrm{sh}}|$ (color online)

In Fig. 9, the convergence of the Burton-Miller CVBEFM is displayed for $k = 1$, π, 2π, 4π, and 8π. Again, the average related error $e(u)$ decreases monotonously and quickly with the decrease in the nodal spacing h, and thus the Burton-Miller CVBEFM is able to produce stable convergence results.

In Table 2, the relative error $|u - u_h|/|u|$ at four points and the average relative error $e(u)$ of the Burton-Miller CVBEFM are displayed for various wavenumbers k. These numerical results are obtained by using $N = 4k$ and $a = 1.0$. We can find from Table 2 that the CVBEFM can produce satisfactory results even for large wavenumbers.

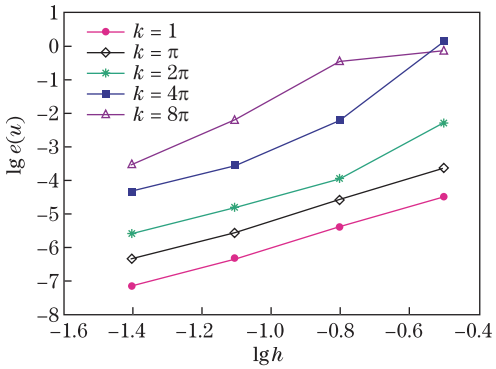

Fig. 9 Results of $e(u)$ at different k for the second example (color online)

Table 2 Errors of the CVBEFM obtained using various k for the second example

Error	Point	k							
		10	20	50	100	200	500	1 000	2 000
$\|u-u_h\|/\|u\|$	$(2.0, \pi/4)$	0.000 91	0.003 02	0.004 56	0.004 56	0.004 57	0.003 83	0.003 46	0.003 34
	$(2.0, 5\pi/8)$	0.001 07	0.000 96	0.001 55	0.000 85	0.000 27	0.000 65	0.000 69	0.000 16
	$(2.0, 7\pi/6)$	0.000 37	0.000 82	0.000 40	0.000 18	0.000 03	0.000 33	0.000 14	0.000 36
	$(2.0, 11\pi/6)$	0.001 83	0.002 24	0.001 98	0.003 03	0.003 50	0.005 05	0.005 68	0.006 65
$e(u)$	–	0.000 86	0.001 77	0.001 51	0.001 35	0.001 28	0.001 20	0.001 22	0.001 25

5.3 Example 3

The third example considers an interior acoustic problem with mixed boundary conditions in a unit circle centered at the origin. Dirichlet and Neumann boundary conditions are imposed on the upper and lower halves of the boundary, respectively. The analytical solution is $u(x_1, x_2) = \sin(\pi x_1)\mathrm{e}^{(\pi^2-k^2)}x_2$.

In Fig. 10, the results of u are presented along the curve given by $x_1 = 0.5\cos\theta$ and $x_2 = 0.5\sin\theta$ with $\theta \in [0, 2\pi]$. The numerical results are obtained by the Burton-Miller CVBEFM using 100 boundary nodes for $k = 10$, 20, and 30. Clearly, the numerical results agree well with analytical results. The convergence is presented in Fig. 11, from which we can see that the method is fast convergent.

6 Conclusions

This paper discusses the meshless numerical analysis of acoustic problems by introducing the Burton-Miller formulation to develop a Burton-Miller CVBEFM for improving the quality of numerical solutions, particularly in the neighborhood of characteristic wavenumbers.

By the utilization of the normal derivative of the solid angle and singularity subtraction procedures, a weakly singular Burton-Miller formulation is derived theoretically to transform both strongly singular and hypersingular integrals into weakly singular integrals. The weakly singular Burton-Miller formulation is valid for both interior and exterior acoustic problems with mixed boundary conditions, admits a unique solution for all wavenumbers, and avoids the computation of the solid angle and its normal derivative. Due to these merits, the CVBEFM is efficient for all wavenumbers, and all integrals in the CVBEFM are at most weakly singular.

In the meshless discretization process of the weakly singular Burton-Miller formulation, the CVMLS approximation is used to approximate unknown boundary variables, which further facilitates the meshless implementation, especially the approximation of boundary variable gradients in the weakly singular Burton-Miller formulation.

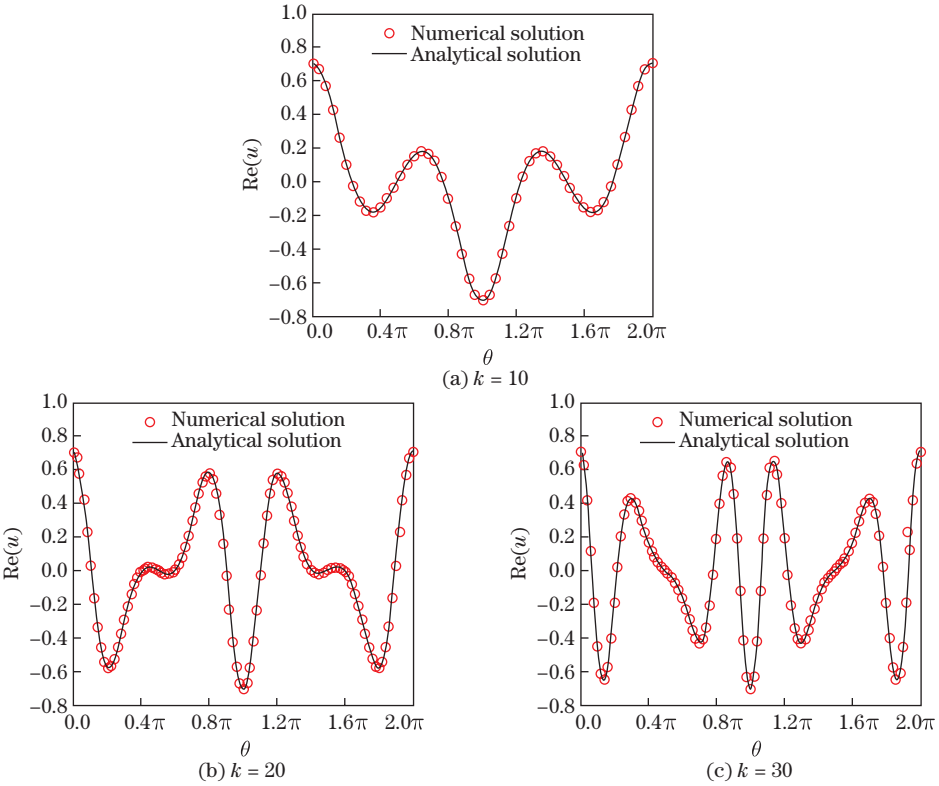

Fig. 10 Real parts of u at different k for the third example (color online)

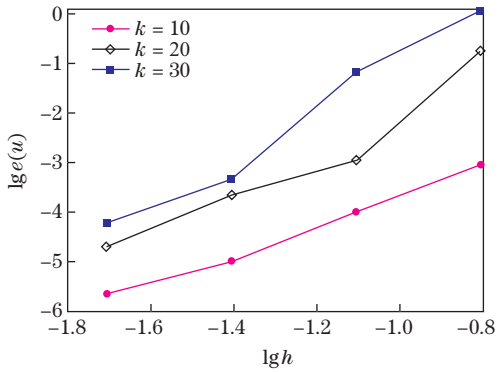

Fig. 11 Results of $e(u)$ at different k for the third example (color online)

Numerical examples testify that the present Burton-Miller CVBEFM only requires boundary nodes and is stable and effective for acoustic problems with arbitrary wavenumbers. Although the performance of meshless methods in previously reported numerical results has been shown mostly for $k < 10$ and seldom for $k \geqslant 100$, this research shows that the present CVBEFM can produce satisfactory results for all wavenumbers, even for extremely large wavenumbers such as $k = 10\,000$.

References

[1] ZHU, J. L. and YUAN, Z. Q. *Boundary Element Analysis*, Science Press, Beijing (2009)

[2] YOUNG, D. L., CHEN, K. H., and LEE, C. W. Singular meshless method using double layer potentials for exterior acoustics. *The Journal of the Acoustical Society of America*, **119**, 96–107 (2006)

[3] CHEN, L. C. and LI, X. L. An improved boundary point interpolation method for exterior acoustic radiation problem. *Engineering Analysis with Boundary Elements*, **103**, 11–21 (2019)

[4] LI, J. P., CHEN, W., FU, Z. J., and QIN, Q. H. A regularized approach evaluating the near-boundary and boundary solutions for three-dimensional Helmholtz equation with wideband wavenumbers. *Applied Mathematics Letters*, **91**, 55–60 (2019)

[5] QU, W. Z., FAN, C. M., GU, Y., and WANG, F. J. Analysis of three-dimensional interior acoustic fields by using the localized method of fundamental solutions. *Applied Mathematical Modelling*, **76**, 122–132 (2019)

[6] WANG, F. J., GU, Y., QU, W. Z., and ZHANG, C. Z. Localized boundary knot method and its application to large-scale acoustic problems. *Computer Methods in Applied Mechanics and Engineering*, **361**, 112729 (2020)

[7] YOU, X. Y., LI, W., and CHAI, Y. B. A truly meshfree method for solving acoustic problems using local weak form and radial basis functions. *Applied Mathematics and Computation*, **365**, 124694 (2020)

[8] WANG, J. R., WU, J. C., and WANG, D. D. A quasi-consistent integration method for efficient meshfree analysis of Helmholtz problems with plane wave basis functions. *Engineering Analysis with Boundary Elements*, **110**, 42–55 (2020)

[9] WU, S. W., XIANG, Y., YAO, J. C., and WANG, S. An element-free Galerkin coupled with improved infinite element method for exterior acoustic problem. *Journal of Theoretical and Computational Acoustics*, **27**, 1850021 (2019)

[10] ANG, W. T. and WANG, X. A numerical method based on boundary integral equations and radial basis functions for plane anisotropic thermoelastostatic equations with general variable coefficients. *Applied Mathematics and Mechanics* (*English Edition*), **41**(4), 551–566 (2020) https://doi.org/10.1007/s10483-020-2592-8

[11] LI, X. L. and LI, S. L. A complex variable boundary point interpolation method for the nonlinear Signorini problem. *Computers and Mathematics with Applications*, **79**, 3297–3309 (2020)

[12] BURTON, A. J. and MILLER, G. F. The application of integral equation methods to the numerical solution of some exterior boundary value problems. *Proceedings of the Royal Society of London A*: *Mathematical and Physical Sciences*, **323**, 201–210 (1971)

[13] CHEN, L. C. and LI, X. L. Boundary element-free methods for exterior acoustic problems with arbitrary and high wavenumbers. *Applied Mathematical Modelling*, **72**, 85–103 (2019)

[14] CHEN, L. C. and LI, X. L. A complex variable boundary element-free method for the Helmholtz equation using regularized combined field integral equations. *Applied Mathematics Letters*, **101**, 106067 (2020)

[15] LIU, G. R., CAI, C., ZHAO, J., ZHENG, H., and LAM, K. Y. A study on avoiding hyper-singular integrals in exterior acoustic radiation analysis. *Applied Acoustics*, **63**, 643–657 (2002)

[16] YAN, Z. Y., CUI, F. S., and HUNG, K. C. Investigation on the normal derivative equation of Helmholtz integral equation in acoustics. *CMES-Computer Modeling in Engineering and Sciences*, **7**, 97–106 (2005)

[17] LI, S. D. and HUANG, Q. B. An improved form of the hypersingular boundary integral equation for exterior acoustic problems. *Engineering Analysis with Boundary Elements*, **34**, 189–195 (2010)

[18] CHENG, Y. M. *Meshless Methods*, Science Press, Beijing (2015)

[19] CHEN, L. C., LIU, X., and LI, X. L. The boundary element-free method for 2D interior and exterior Helmholtz problems. *Computers and Mathematics with Applications*, **77**, 846–864 (2019)

[20] LI, X. L. and LI, S. L. Analysis of the complex moving least squares approximation and the associated element-free Galerkin method. *Applied Mathematical Modelling*, **47**, 45–62 (2017)

[21] VIDELA, J., ANITESCU, C., KHAJAH, T., BORDAS, S. P., and ATROSHCHENKO, E. h- and p-adaptivity driven by recovery and residual-based error estimators for PHT-splines applied to time-harmonic acoustics. *Computers and Mathematics with Applications*, **77**, 2369–2395 (2019)

[22] MARBURG, S. The Burton and Miller method: unlocking another mystery of its coupling parameter. *Journal of Computational Acoustics*, **24**, 1550016 (2016)

[23] ZHANG, T. and LI, X. L. Analysis of the element-free Galerkin method with penalty for general second-order elliptic problems. *Applied Mathematics and Computation*, **380**, 125306 (2020)

[24] XIE, D., JIAN, K., and WEN, W. Global interpolating meshless shape function based on generalized moving least-square for structural dynamic analysis. *Applied Mathematics and Mechanics* (*English Edition*), **37**(9), 1153–1176 (2016) https://doi.org/10.1007/s10483-016-2126-6

[25] WEI, C. Q., YAN, Z. Z., ZHENG, H., and ZHANG, C. Z. RBF collocation method and stability analysis for phononic crystals. *Applied Mathematics and Mechanics* (*English Edition*), **37**(5), 627–638 (2016) https://doi.org/10.1007/s10483-016-2076-8

[26] LI, X. L. and DONG, H. Y. Error analysis of the meshless finite point method. *Applied Mathematics and Computation*, **382**, 125326 (2020)

[27] ZHANG, T. and LI, X. L. Variational multiscale interpolating element-free Galerkin method for the nonlinear Darcy-Forchheimer model. *Computers and Mathematics with Applications*, **79**, 363–377 (2020)

[28] QU, W. Z., FAN, C. M., and LI, X. L. Analysis of an augmented moving least squares approximation and the associated localized method of fundamental solutions. *Computers and Mathematics with Applications*, **83**, 13–30 (2020)

[29] MA, J. J., ZHU, J. L., and LI, M. J. The Galerkin boundary element method for exterior problems of 2-D Helmholtz equation with arbitrary wavenumber. *Engineering Analysis with Boundary Elements*, **34**, 1058–1063 (2010)

[30] CHEN, J. T., CHEN, C. T., CHEN, P. Y., and CHEN, I. L. A semi-analytical approach for radiation and scattering problems with circular boundaries. *Computer Methods in Applied Mechanics and Engineering*, **196**, 2751–2764 (2007)